Chemical Science

EDGE ARTICLE

View Article Online
View Journal | View Issue

Cite this: *Chem. Sci.*, 2018, **9**, 2348

A combined experimental and computational study on the reaction of fluoroarenes with Mg–Mg, Mg–Zn, Mg–Al and Al–Zn bonds†

Clare Bakewell, Bryan J. Ward, Andrew J. P. White and Mark R. Crimmin *

Through a combined experimental and computational (DFT) approach, the reaction mechanism of the addition of fluoroarenes to Mg–Mg bonds has been determined as a concerted S_NAr-like pathway in which one Mg centre acts as a nucleophile and the other an electrophile. The experimentally determined Gibbs activation energy for the addition of C_6F_6 to a Mg–Mg bond of a molecular complex, $\Delta G^{\ddagger}_{298\ K}$(experiment) = 21.3 kcal mol^{-1} is modelled by DFT with the ωB97X functional, $\Delta G^{\ddagger}_{298\ K}$(DFT) = 25.7 kcal mol^{-1}. The transition state for C–F activation involves a polarisation of the Mg–Mg bond and significant negative charge localisation on the fluoroarene moiety. This transition state is augmented by stabilising closed-shell Mg···F_{ortho} interactions that, in combination with the known trends in C–F and C–M bond strengths in fluoroarenes, provide an explanation for the experimentally determined preference for C–F bond activation to occur at sites flanked by *ortho*-fluorine atoms. The effect of modification of both the ligand coordination sphere and the nature and polarity of the M–M bond (M = Mg, Zn, Al) on C–F activation has been investigated. A series of highly novel β-diketiminate stabilised complexes containing Zn–Mg, Zn–Zn–Zn, Zn–Al and Mg–Al bonds has been prepared, including the first crystallographic characterisation of a Mg–Al bond. Reactions of these new M–M containing complexes with perfluoroarenes were conducted and modelled by DFT. C–F bond activation is dictated by the steric accessibility, and not the polarity, of the M–M bond. The more open coordination complexes lead to enhanced Mg···F_{ortho} interactions which in turn lower the energy of the transition states for C–F bond activation.

Received 25th November 2017
Accepted 19th January 2018

DOI: 10.1039/c7sc05059c

rsc.li/chemical-science

Introduction

The activation of strong carbon–fluorine bonds remains a key academic and industrial challenge that is motivated by the prevalence of fluorine-containing molecules in the pharmaceutical, agricultural and materials industries. Recent advances have focused on the functionalisation of fluoroarenes, with aim of making synthetically useful building blocks.[1,2] In particular, C–F activation and subsequent borylation has been reported to occur catalytically using a range of late transition metal catalysts.[3–13]

The activation of aromatic sp^2 C–F bonds with transition metal complexes is known to proceed by several mechanisms, most common of which are oxidative addition (OA) and nucleophilic aromatic substitution (S_NAr).[14–16] Oxidative addition is typically observed with 14- or 16-electron complexes of the form ML_2 (M = Ni, Pd, Pt) or ML_3X (M = Rh, Ir), where higher oxidation states are easily accessible.

The concept of ligand-assisted C–F bond activation was introduced to rationalise experimentally observed fluorophosphines, formed during the reaction of perfluoroarenes with group 9 and 10 transition metal phosphine complexes.[17,18] Originally reported by Milstein in the early 1990s, the reaction of C_6F_6 with $[(Et_3P)_3IrMe]$ forms $[(Et_3P)_2(FEt_2P)IrC_6F_5]$ along with ethene and methane. Density functional calculations were used to substantiate a pathway that occurs by 1,2-addition of the C–F to the Ir–P bond: nucleophilic attack of the electron-rich metal on the fluorocarbon occurs with simultaneous activation, and trapping, of the fluoride by the phosphine. The concept has been expanded to boryl-assisted C–F activation using a $[(Et_3P)_3RhBpin]$ complex and the mechanism used to explain the experimentally observed activation of pentafluoropyridine at the 2-position (Fig. 1 – ligand assisted OA).[3]

Lewis acid-assisted C–F bond activation, has been explored in a detailed experimental and theoretical study by Nakamura and co-workers. This mechanism is conceptually related to the ligand-assisted pathway but differs in that the Lewis acidic and nucleophilic metal centers are not directly bound to one

Department of Chemistry, Imperial College London, South Kensington, London, SW7 2AZ, UK. E-mail: m.crimmin@imperial.ac.uk

† Electronic supplementary information (ESI) available: Experimental procedures, details of the DFT studies, single crystal X-ray data and multinuclear NMR spectra (DOI: 10.14469/hpc/3155). X-ray crystallographic data for **2a**, **2a–hexane**, **2b**, **3**, **3·THF**, **3a**, **4**, **6** and **7** (CIF). CCDC 1575549–1575558, 1577209. For ESI and crystallographic data in CIF or other electronic format see DOI: 10.1039/c7sc05059c

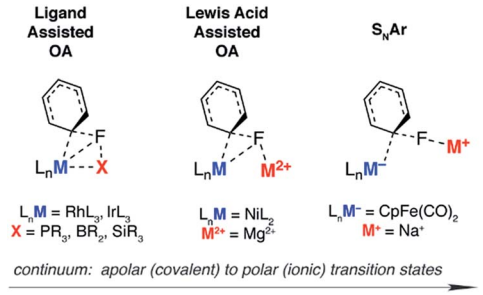

Fig. 1 Selected transition states for C–F bond activation of fluoroarenes.

another (Fig. 1 – Lewis acid assisted OA). Kumada–Tamao–Corriu cross-coupling reactions between aryl fluorides and Grignard reagents can be catalysed by [Ni(acac)$_2$].[19] The use of a dinucleating hydroxyphosphine ligand leads to an active catalyst, which operates through a cooperative push–pull mechanism. The nickel and magnesium centers act as electron donors and acceptors respectively, facilitating C–F bond activation.

Nucleophilic mechanisms have been invoked for coordinatively saturated anionic 18-electron complexes, and are facilitated by the highly polar C–F bond. For example, C–F activation of fluoroarenes and fluoroalkenes using the Fp$^-$ (cyclopentadienyliron dicarbonyl) anion is proposed to occur by nucleophilic aromatic substitution (Fig. 1 – S$_N$Ar) and nucleophilic vinylic substitution respectively.[20,21] While the relative rates of reactions are consistent with the known nucleophilicity scale[20] of anionic transition metal carbonyl complexes,[22,23] the true degree of charge separation in the proposed transition state for C–F bond activation remains a point of debate.[24] Related nucleophilic anionic intermediates, formed *via* deprotonation of [Cp*M(PMe$_3$)H$_2$] (M = Rh, Ir) are also postulated to be the active species in C–F bond activation reactions.[25,26]

We recently reported the C–F bond activation of a series of perfluorinated and partially fluorinated arenes, using the low valent Mg(I) species **1** (Fig. 2).[27,28]

The reaction results in the formation of a new Mg–C bond and a new Mg–F bond and may be considered as a homogeneous equivalent to Grignard formation. The new organometallic complexes have potential to be used as fluorinated building blocks in synthesis.[29] Initial mechanistic investigations provided support for a concerted two-electron reaction

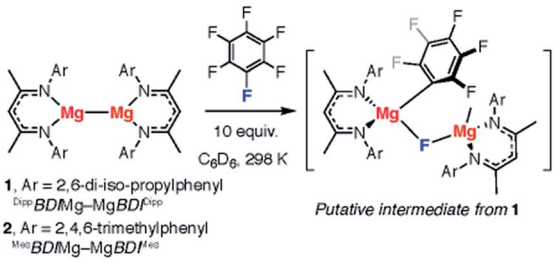

Fig. 2 C–F bond activation of fluoroarenes using Mg–Mg reagents.

pathway, with no radical intermediates detected through trapping experiments. A plausible transition state for this reaction involves the 1,2-addition of the C–F bond across the apolar Mg–Mg bond.

Herein, we report a joint experimental and computational analysis of the carbon–fluorine bond activation of fluorinated arenes using low-valent complexes which contain M–M bonds (M = Mg, Zn, Al). We provide strong evidence for the proposed concerted pathway and a transition state reminiscent of those represented in Fig. 1 that involves dual nucleophilic and electrophilic sites that polarise and activate the C–F bond. We introduce additional experiments and prepare new M–M complexes in order to interrogate the key transition state for C–F activation. Specifically, the effects of steric accessibility and M–M bond polarity on reaction rates are reported.

Results

Concerted addition of C_6F_6 to 1

The reaction mechanisms reported herein were studied by DFT using the Gaussian 09 suite (revision D.01)[30] and optimisations employed the ωB97X functional.[31] Mg and Zn centers were described with Stuttgart SDDAll RECPs and associated basis sets whereas 6-31G** basis sets was used for all other atoms.[32–36] Free energies are corrected for both benzene solvent using the Polarisable Continuum Model (PCM) approach and dispersion effects using ωB97X-D.[37,38]

The potential energy surface for the reaction of C_6F_6 with **1** is presented in Fig. 3a. C–F bond activation is initiated upon weak coordination of C_6F_6 to the ligand sphere of 1 to create the encounter complex, **Int-A**. Substrate association to **1** occurs by a network of non-covalent interactions (*e.g.* C–H···F, C–H···π, π···π) which although individually weak contribute to a modest binding enthalpy of $\Delta H^o = -9.2$ kcal mol^{-1} (Fig. S27†).

The increased ordering of the system is, however entropically unfavourable and thus fluoroarene binding is slightly endergonic ($\Delta G^o = 1.1$ kcal mol^{-1}). The ligands in **Int-A** are oriented perpendicular to one another and rotation around the Mg–Mg bond is required to access the more reactive conformer **Int-A′**. **Int-A′** contains a reactive pocket and a sterically accessible Mg–Mg bond. C–F bond activation occurs *via* the concerted transition state **TS-1** ($\Delta G^{\ddagger}_{298\ K} = 25.7$ kcal mol^{-1}). Decay from **TS-1** leads to the C–F activation product **Int-B** in which a newly formed Mg–C bond and bridging Mg–F–Mg bond contribute to a 6-membered ring structure. Overall C–F bond activation is extremely exergonic ($\Delta G^o_{rxn} = -112.2$ kcal mol^{-1}).

An Eyring analysis on the reaction of **1** with C_6F_6 under pseudo first-order conditions, conducted over the temperature range 258–288 K, yielded activation parameters $\Delta H^{\ddagger} = 10.8$ kcal mol^{-1} and $\Delta S^{\ddagger} = -35$ cal K^{-1} mol^{-1} (Fig. 3b and c). The experimental negative activation entropy is consistent with a highly ordered transition state, while the activation enthalpy is suggestive of a transition state with only minimal bond making and breaking having occurred. The Gibbs activation energy $\Delta G^{\ddagger}_{298\ K} = 21.3$ kcal mol^{-1} matches reasonably well with that determined from DFT, $\Delta G^{\ddagger}_{298\ K} = 25.7$ kcal mol^{-1}.[39]

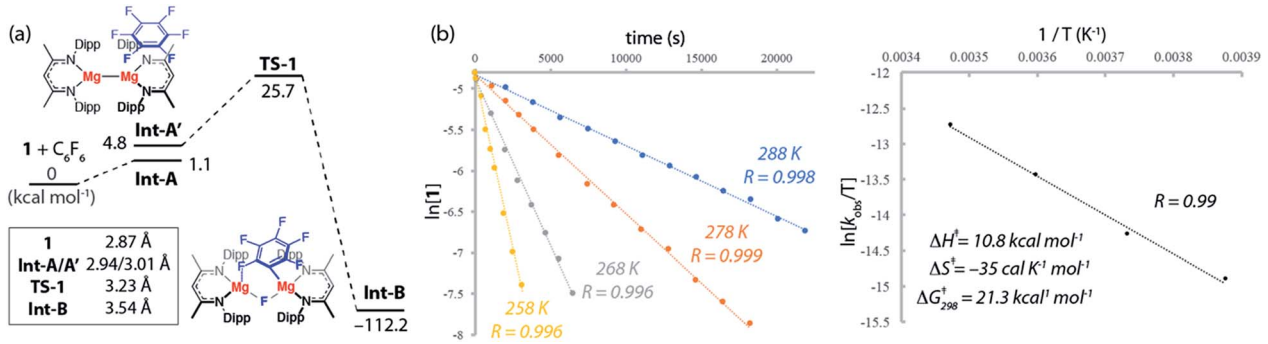

Fig. 3 (a) The calculated reaction pathway for C–F activation with **1**, inset shows Mg···Mg separation. (b) Kinetics of the reaction of **1** with 10 equiv. of C_6F_6 at various temperatures and Eyring analysis with determined activation parameters for C–F activation.

The transition state for C–F bond activation

The calculated **TS-1** is suggestive of an asynchronous concerted process: considerable Mg–C bond formation has occurred before any significant C–F bond breaking (Fig. 4). Formally, the transition state involves the concerted oxidative addition of the C–F bond to the Mg–Mg bond. Related pathways have been calculated for the addition of C–F bonds of fluoroarenes to single-site Al(I) and Si(II) centres.[40–42] The bond lengths and angles around the *ipso*-carbon (Fig. S28a†), along with the charge distribution about the aromatic ring, however are consistent with an S_NAr-like mechanism for C–F activation with one Mg center acting as a nucleophile, attacking the aromatic ring, while the other acts as an electrophile, binding to and polarising the breaking C–F bond.

An electron density difference map illustrates the depletion of electron density between the breaking C–F and Mg–Mg bonds along with the simultaneous accumulation of electron density between Mg and C at the forming Mg–C bond (Fig. 4a). Electron density accumulation also occurs at both *ortho*- and *para*-carbons of the fluoroarene. The electron density redistribution in **TS-1** is mirrored by the NBO analysis showing the difference in the NPA charges between **TS-1** and **Int-A′** (Fig. 4b). The loss of electron density at the Mg centers ($\Delta = +0.52$ e) is redistributed to the fluoroarene ring ($\Delta = -0.53$ e) and approximately half of the redistributed electron density is localised at *ipso*-carbon ($\Delta = -0.27$ e).

The effect of functional group substitution on the reaction rates of concerted S_NAr pathways is well understood: stabilisation of the negative charge on aromatic ring through inductive and mesomeric effects leads to an increase in reaction rate. Rate constants were measured for the reaction of **1** with a series of fluoroarenes of the form C_6F_5R. The group *para*- to the breaking C–F bond was varied and rate constants were measured under pseudo first-order conditions (Table S1†). Broadly the relative rate increases with stabilisation of negative charge on the *ipso*-carbon, leading to the general reactivity trend: R = CF_3 > F > C_6F_5 > CH_3.

Importance of secondary Mg···F_{ortho} interactions in the TS for C–F activation

In addition to the expected Mg···F_{ipso} interaction derived from the breaking C–F bond, there is a significant Mg···F_{ortho} interaction in **TS-1** that is retained in **Int-B**. The presence of a strong Mg···F_{ortho} interaction is evidenced by a short Mg···F_{ortho} distance (2.34 Å). The QTAIM molecular graph of **TS-1** (Fig. 4c) identifies the presence of a bond critical point (BCP) between

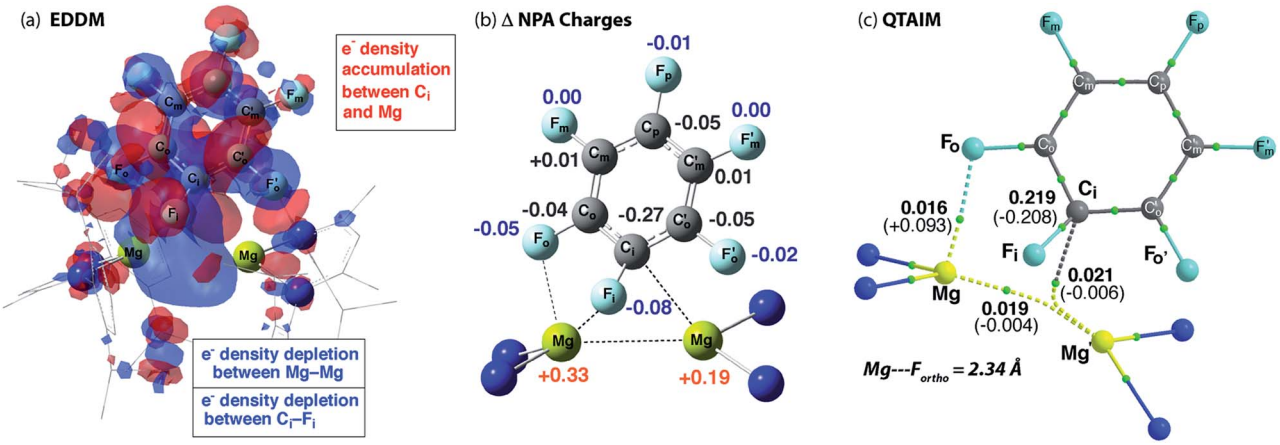

Fig. 4 (a) Energy density difference map (EDDM) for **TS-1**, (b) the change (Δ) in NPA charges from **Int-A′** to **TS-1** and (c) QTAIM data on **TS-1**: $\rho_{(r)}$ values in bold, $\nabla^2\rho$ values in parentheses. Full QTAIM for **TS-1** in Fig. S28b.†

Mg and F_{ortho}. The attributes of the BCP (small $\rho_{(r)}$, small positive $\nabla^2\rho$) are indicative of a weak, closed shell interaction. The DFT prediction of this secondary Mg···F interaction is particularly noteworthy, as experimentally the addition of C–F bonds of fluoroarenes to the Mg–Mg bond of **1** always proceeds to give regioisomers in which at least one *ortho*-fluorine atom is adjacent to the C–F bond that breaks.

The effect of the position of fluorine substitution and the importance of the secondary Mg···F_{ortho} interaction on the C–F bond cleavage transition state was interrogated by calculating the pathway for the addition of C_6F_5H to **1**. Fig. 5 compares the change in Gibbs activation energy for the regioisomeric transition states (relative to **TS-1**). DFT calculations predict that substitution at positions X^2 and X^3 should lead to lowest energy transition states. Experimentally, regioisomeric products of C–F activation of both these positions of C_6F_5H are observed.[27]

Substitution (of fluorine for hydrogen) at X^1 is highly disfavored and removes the *ortho*-fluorine substituent that anchors the substrate in the C–F bond activation TS ($\Delta\Delta G$ = +5.1 kcal mol^{-1}). For comparison, X^5 is not involved in appreciable Mg···F_{ortho} bonding in the transition state and substitution here only raises the TS by +1.8 kcal mol^{-1}. Substitution at X^4 also raises the energy of the C–F activation TS ($\Delta\Delta G$ = +2.8 kcal mol^{-1}). This position is expected to exert a secondary influence on the Mg···F_{ortho} binding energy. The fluorine atom in position X^4 is a weak π-donor and will increase the electron density on X^1. Replacing X^4 with a hydrogen atom will remove this effect diminishing the electrostatic interaction between Mg and F_{ortho}.

The importance of the *ortho*-fluorine substituents was further exemplified by calculating the transition state for C–F bond activation of 1,3-$C_6F_4H_2$ in which both positions *ortho*- to the breaking C–F bond are occupied by hydrogen atoms (Fig. S30†). The absence of any Mg···F_{ortho} anchor results in a reorganisation of the TS to a conformer in which the breaking C–F bond is parallel with the Mg–Mg bond ($\Delta\Delta G$ = +9.5 kcal mol^{-1} relative to **TS-1**). The geometry of this reorganised TS is consistent with that reported for the addition of CO_2 to **1** reported by Maron and co-workers.[43]

Effect of sterics on the TS for C–F activation

A number of analogues of **1** are known. These include a series of β-diketiminate complexes which differ in the steric profile of the flanking aromatic groups on the ligand. Consideration of the data above leads to the obvious question, what are the effects of sterics in C–F bond activation by addition to a Mg–Mg bond?

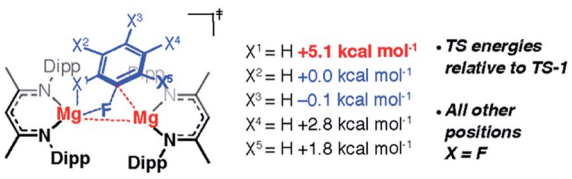

Fig. 5 Effect of H-atom regiochemistry in the TS for C–F activation of C_6F_5H.

The potential energy surface for C–F bond activation of C_6F_6 by **2** (^{Mes}BDIMg–MgBDI^{Mes}) was calculated and compared to that of **1** (^{Dipp}BDIMg–MgBDI^{Dipp}). The reduced steric bulk of the mesityl substituents results in greater access to the Mg–Mg bond. Consequently, the substrate coordinates to Mg in **2** through a short Mg···F interaction (2.76 Å) to give **Int-C**. Overall, the formation of **Int-C** is facile (ΔG = 0.3 kcal mol^{-1}). Rotation about the Mg–Mg bond in **Int-C** gives the more reactive conformer **Int-C′** which contains a stronger Mg···F interaction (2.66 Å) in the form of a κ^1-bound fluoroarene adduct.[44,45] The transition state for C–F cleavage **TS-2** is located 23.0 kcal mol^{-1} above the reactants and leads to **Int-D** (Fig. 6a). Significantly **TS-2** contains two Mg···F_{ortho} interactions as evidenced by the short M···F_{ortho} distances (Fig. S31a†) and quantified by QTAIM analysis (Fig. 6b). These electrostatic interactions undoubtedly contribute to transition state stabilisation and explain the lower energy of **TS-2** relative to **TS-1** (Fig. 6a).

Experimental data were collected to verify the hypothesis that **2** is more reactive to fluoroarenes than **1** (Fig. 6c). The reaction between **2** (0.02 M) and 10 equiv. of C_6F_6 in C_6D_6 was facile, with immediate observation of ^{19}F NMR resonances at δ = −118.5, −157.1 and −158.3 ppm corresponding to the Mg–C_6F_5 moiety. A further resonance at δ = −183.3 ppm is assigned to a Mg–F by-product.[46] A competition reaction between **1**, **2**, and C_6F_6, led exclusively to products derived from C–F bond activation with **2**. Further experiments replacing C_6F_6 with 2-(2,3,4,5,6-pentafluorophenyl)-pyridine (2-Py-C_6F_5) again led to exclusive reaction of **2** with no evidence for the participation of **1** despite its known reaction with the same substrate. As with the analogous reaction using **1**, **2** reacts with 2-Py-C_6F_5 at the 2-position. Both the C–F activation product **2a** and the fluoride-containing by-product [{^{Mes}BDIMg}$_3$(μ-F)$_3$] (**2b**) have been characterised by single crystal X-ray diffraction, the latter complex forming a fluoride bridged trimer in the solid state.[47]

Effect of M–M bond polarisation on the TS for C–F activation

The polarisation of the Mg···Mg bond in **TS-1** and **TS-2** raises a further question: do reactions of polar M–M bonds proceed faster than apolar M–M bonds? To address this question a series of new heterobimetallic complexes with polar M–M′ bonds (M = Mg, M′ = Zn, Al; M = Zn, M′ = Al) were prepared. Complexes **3**, **4**, **6**, **7** are novel M–M containing species, and their synthesis was inspired by recently described methods, namely metathesis,[48–52] and insertion of an Al(I) reagent[53–59] into metal–carbon bonds.[60,61] Despite the exploitation of known methods, this represents a highly novel series of main group complexes containing metal–metal bonds, including the first example of a crystallographically characterised Mg–Al bond and rare examples of Mg–Zn, Zn–Al and Zn–Zn–Zn bonds for which there is limited precedent.

Complex **3**, containing a new Mg–Zn bond, was synthesised by the stoichiometric reaction of the corresponding zinc iodide with **2** (Scheme 1). The reaction occurs with concomitant formation of one equiv. of the β-diketiminate supported magnesium(II) iodide and **3** could be isolated cleanly by exploitation of the difference in solubility between the two products (54%

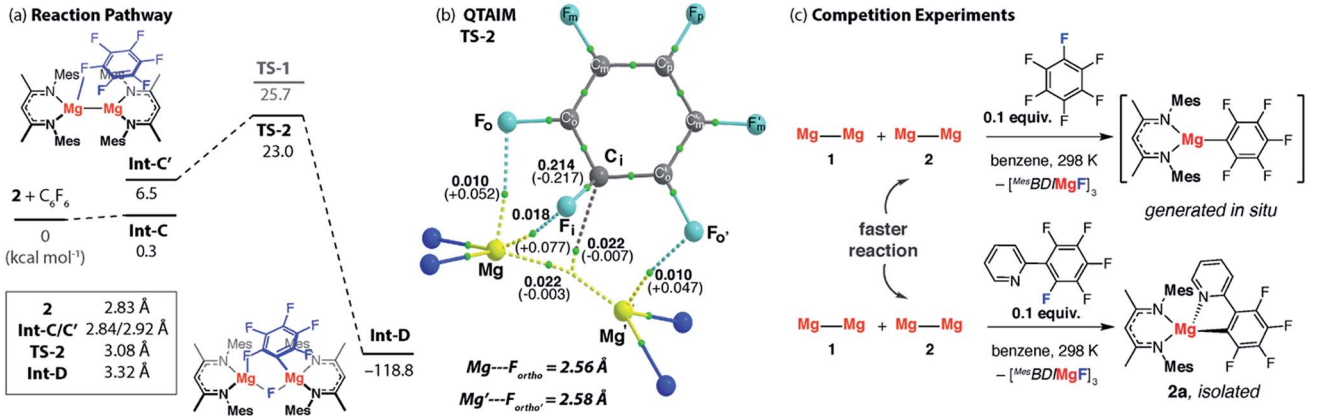

Fig. 6 (a) The calculated reaction pathway for C–F activation with **2**, inset shows Mg···Mg separation. (b) QTAIM plot of **TS-2**: $\rho_{(r)}$ values in bold, $\nabla^2\rho$ values in parentheses. Full QTAIM for **TS-2** in Fig. S31b.† (c) Competition experiments between **1** or **2** and fluoroarenes.

isolated yield). Compound **3** was found to be unstable in solution, degrading slowly over time (days) to form the mixed bis-β-diketiminate complex [Mg(DippBDI)(MesBDI)] along with a black precipitate (presumed to be Zn^0). Compound **3** can, however, be stored over a prolonged period of time at 238 K, as a solid or in hydrocarbon solution. This complex may be trapped by insertion of a carbodiimide (RN=C=NR, R = Cy, i-Pr) into the Mg–Zn bond and details of these experiments are provided in the ESI.† An analogue of **3** bearing solely mesityl substituted ligands was also prepared but could not be isolated cleanly.

X-ray quality crystals of **3** were grown from *n*-hexane at 238 K. The Mg–Zn bond length in **3** is 2.5993(8) Å, which is comparable with the only two previously reported examples of complexes containing a magnesium–zinc bond (Fig. 7, Table 1).[48] This value lies between the bond lengths of analogous Mg–Mg (2.8078–2.8700(9) Å) and Zn–Zn (2.3586(7)-2.3813(8) Å) β-diketiminate complexes.[27,51,62–64] Comparison of the series of structures reveals that the complexes adopt a number of conformers in the solid state which differ by the dihedral angle between the two β-diketiminate planes. A low energy difference between these conformers is anticipated, as would be consistent with the small calculated energy difference between **Int-A** and **Int-A′** (Fig. 3).

Addition of the coordinating solvents, THF and pyridine, to **3** led to the formation of the coordination complexes **3·THF** and **3·Py**, respectively. Integration of the ^{1}H NMR spectra indicates that in both cases only one equiv. of solvent is bound (Scheme 1). This was confirmed by the X-ray structure of **3·THF**, which shows one molecule of tetrahydrofuran coordinated to magnesium, whilst the zinc remains in a three-coordinate geometry (Fig. 7).

The Mg–Zn bond length of **3·THF** (2.6816(8) Å) is significantly longer than that of **3**, a phenomenon also observed in the di-solvated solid-state structures of **1** (where solv. = THF, pyridine, DMAP).[65] **3·THF** is a loose approximation of **Int-C′** (Fig. 6a) and suggests that substrate coordination to a single metal center is a feasible proposition in the pathway for C–F bond activation.

Following isolation of **3**, further small amounts of bright yellow crystals were observed to form in the reaction filtrate. Single crystal X-ray diffraction revealed formation of the novel tri-zinc species, **4**. Compound **4** is only the second reported example of a linear tri-zinc complex.[48] **4** is C_i symmetric and the Zn–Zn–Zn bond is linear (180°). The Zn–Zn bond length of 2.3908(3) Å is slightly longer than in the previously reported example bearing mono-dentate amide ligands. Compound **4** is iso-structural with a previously reported Zn–Hg–Zn complex.[52,66]

Related Mg–Al and Zn–Al complexes were also prepared. The stoichiometric reaction of **5** with magnesium and zinc alkyl complexes in C_6D_6 resulted in the formation of new asymmetric products, **6** and **7**, respectively (Scheme 1). Deep red crystals of **6** and yellow crystals of **7** were grown from concentrated *n*-hexane solutions at 238 K (Fig. 7). Single crystal X-ray diffraction studies confirmed the presence of a newly formed aluminium–metal bond, which measured 2.7687(5) Å for Al–Mg and 2.488(1) Å for Al–Zn.[60] The aluminium centers in **6** and **7** have a distorted tetrahedral geometry, with τ'_4 values of 0.87 and 0.93, respectively. Both compounds **6** and **7** were found to be remarkably

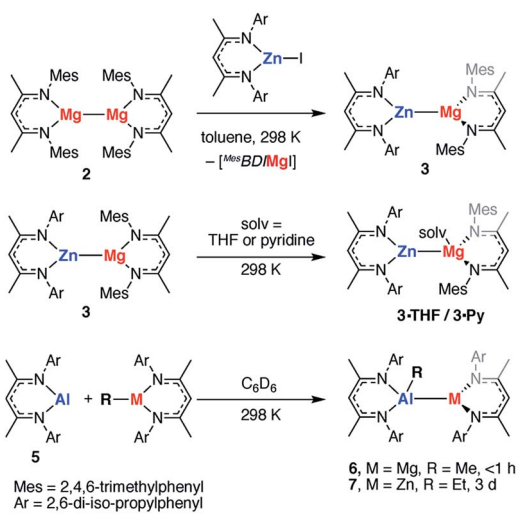

Scheme 1 Preparation of polar M–M heterobimetallics.

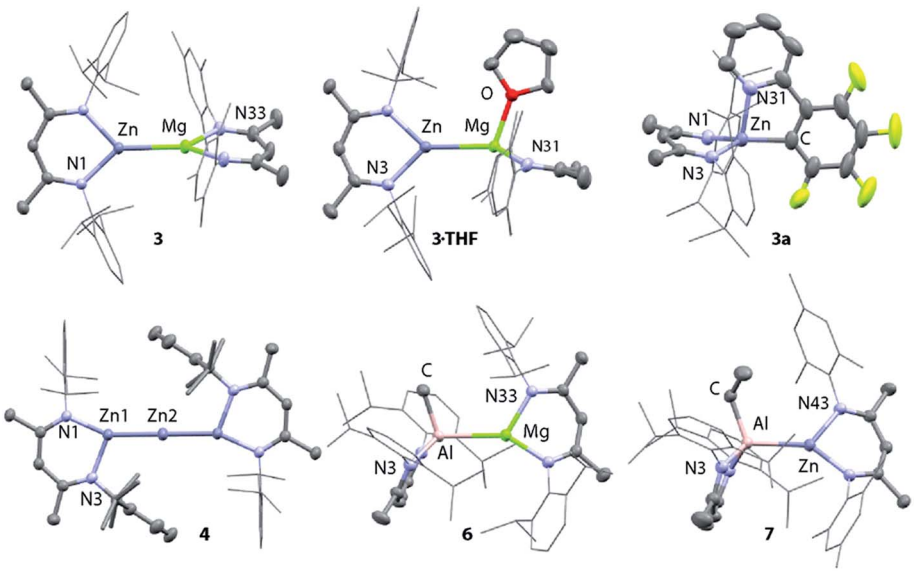

Fig. 7 The crystal structures of **3**, **3**·THF, **3a**, **4**, **6** and **7**.

stable in solution, with no degradation observed when heated for 48 h at 353 K.[67]

The effect of polarity on C–F activation with main group compounds containing M–M′ bonds was investigated. Reaction of the heterobimetallic species **3**, **6** and **7**, with fluoroarenes were conducted in hydrocarbon solution. No evidence of C–F bond activation was observed upon reaction of Mg–Al (**6**) or Zn–Al (**7**) containing compounds with a range of fluorocarbons (*e.g.* C_6F_6, C_6F_5H and 2-Py-C_6F_5) between 298 and 353 K. While **3** does react slowly with C_6F_6 at room temperature this reaction is competitive with decomposition of the Mg–Zn reagent.[68,69] A clean reaction was observed between **3** and 2-Py-C_6F_5 to form the Zn complex **3a** and the corresponding magnesium fluoride (Scheme 2, Fig. 7).

The reaction pathway for the addition of C_6F_6 to **3** was calculated and shown to be analogous to that described for **1**. C–F bond cleavage occurs *via* an asymmetric transition state **TS-3** (Fig. S32†) which leads to Zn–C and Mg–F bond formation and is 26.4 kcal mol^{-1} higher in energy than the separated reactants. Consideration of the difference in electronegativity between Mg (χ_p = 1.31) and Zn (χ_p = 1.65) explains the geometry of the transition state and the destination of the fluorine atom in the reaction. All attempts to locate a transition state that resulted in Mg–C and Zn–F bond formation led to **TS-3** and it is clear that polarisation of the M–M′ bond is a key factor in determining the outcome of the reaction (Fig. 8a).

In combination, these experiments suggest that Mg–Zn, Mg–Al and Zn–Al reagents prepared herein are all less reactive toward fluoroarenes than **1** or **2**. This finding was borne out by competition experiments using both C_6F_6 and 2-Py-C_6F_5. The rate of reaction of **3** with 2-Py-C_6F_5 is marginally slower than

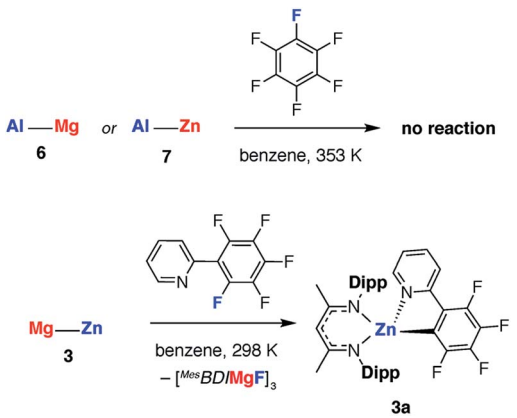

Scheme 2 Reactions of polar M–M bonds with fluoroarenes.

Table 1 Selected bond lengths from the X-ray data of **3**–**7**[a]

	3	3·THF	2a	3a	4	6	7
M–M	2.5993(8)	2.6816(8)	—	—	2.3908(3)	2.7687(8)	2.4877(10)
fsr	0.99	1.03	—	—	0.98	1.06	1.00
M–N	2.0243(18)	2.0782(19)	2.037(3)	1.979(2)	1.9761(18)	2.0862(10)	2.034(3)
	2.0540(19)	2.0999(19)	2.035(3)	1.973(2)	2.016(3)	1.9739(10)	1.933(3)
M–X	—	2.1116(18)	2.156(4)	1.980(3)	—	1.9856(13)	1.980(3)
		X = O	X = C	X = C		X = C	X = C

[a] fsr is the formal shortness ratio defined as the bond length/sum of the single bond radii (Pauling).

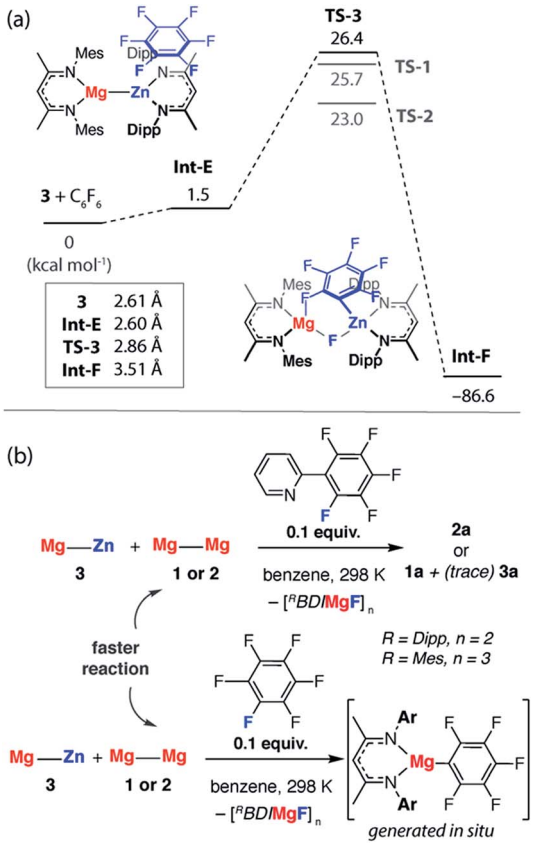

Fig. 8 (a) The calculated reaction pathway for C–F activation with **3**. (b) Competition experiments.

with **2**, $t_{1/2} = 1$ h *versus* <0.5 h, but is significantly faster than degradation of **3**. Competition experiments between **3** and **2** confirm the relative rates and led to reaction of the Mg–Mg reagents in all cases (Fig. 8b). While competition experiments between **3** and **1** also resulted in selective formation of the organomagnesium species, in this instance trace amounts of **3a** are also formed. The relative reactivity is predicted by DFT calculations and **TS-3** is higher in energy than both **TS-2** ($\Delta\Delta G =$ 3.4 kcal mol^{-1}) and **TS-1** ($\Delta\Delta G =$ 0.7 kcal mol^{-1}). Given the small energy difference involved, the computational methods do not result in a quantitative prediction of the reaction outcome in terms of an accurate product distribution but rather a qualitative prediction of the most reactive species. In line with these predictions, C–F bond activation by **6** and **7** are calculated to occur by concerted transition states **TS-4** and **TS-5** (Fig. S33†) with $\Delta G^{\ddagger}_{298\ K}$ of 40.0 and 65.1 kcal mol^{-1} respectively. While in both cases the calculations predict the formation of C–Al bonds upon C–F activation with **6** or **7**, the activations barriers are prohibitively high and these reactions are not observed experimentally.

Conclusions

Sterics *versus* bond polarisation

Comparison of **TS-1-3** and consideration of the competition experiments definitively shows that sterics are the dominant factor at play in determining the reactivity of M–M bonds toward C–F activation of fluoroarenes. Despite polarisation of the M–M bond occurring in the transition state to C–F bond cleavage, introduction of polarity into the M–M′ bond by variation of the metals, while determining the selectivity of addition, does not lead to faster rates of reaction. Moreover, blocking access to the M–M′ bond through increasing the coordination number of one of the metals from 3- to 4-coordinate (in **6** and **7**) completely shuts down reactivity. These results can be rationalised based on the ease of the formation of the C–F bond activation transition state. The polar heterobimetallics (such as **3**) have contracted M–M′ bonds relative to apolar ones, due to the ionic contribution to bonding, and this bond length contraction closes up the steric pocket that is required for formation of the transition state for C–F bond activation (Table S7, Fig. S34†).

A thermodynamic *ortho*-fluorine influence and kinetic *ortho*-fluorine effect

In our initial communication of this work, we showed that C–F bond activation with **1** occurs at positions that are flanked by at least one *ortho*-fluorine substituent.[27] Substrate control of regioselectivity is rigorously enforced in these systems and an *ortho*-fluorine substituent appears essential for the reactions to proceed.

Reactivity trends of fluorinated arenes with transition metal complexes are increasingly well understood in both qualitative and quantitative terms.[1,5,70,71] Experimentally, the activation of C–F bonds becomes kinetically more challenging as the number of fluorine atoms in $C_6F_nH_{6-n}$ decreases.[27] The influence of fluorine substitution on C–M bond strengths has been the subject of numerous studies. The C–M bond strength increases with an increasing number of *ortho*-fluorine substituents and this phenomenon is in part accountable for the "*ortho*-fluorine effect" in reactions that break C–H bonds of fluoroarenes.

Whittlesey and Macgregor have calculated the influence of substitution patterns on the properties of fluoroarenes and found that substituting hydrogen for fluorine decreases C–F bond strengths in the order *ortho*- > *meta*- > *para*-.[72] Hence, there is a clear thermodynamic rationale for C–F bond activation with M–M reagents to occur at positions flanked by one or more fluorine substituents. These positions are likely to have the weakest C–F bonds and lead to the formation of strongest C–M bonds.

Consideration of **TS-1-3** reveals that a kinetic factor also needs to be considered. M···F_{ortho} fluorine interactions are not only present in the key transition states for C–F bond activation, they determine the geometry of these transition states and significantly lower their energy. The role of electrostatic M···F bonding in C–F bond activation with organocerium complexes by a 'harpoon mechanism' has been highlighted by Maron and coworkers.[73] Furthermore, Whittlesey and Macgregor have also commented on the effect of *ortho*-fluorine substitution on stabilising transition states during concerted C–F bond activation with transition metal complexes.[72] To clarify the dual role of *ortho*-fluorine substitution in the reaction pathways reported

herein we suggest that C–F bond activation by M–M reagents could be best described as being subject to:

(i) an *ortho*-fluorine influence that results in destabilisation of the starting materials and stabilisation of the reaction products due to weakened C–F bond strengths and increased M–C bond strengths.

(ii) an *ortho*-fluorine effect that results in a rate-acceleration through stabilisation of the transition state for C–F bond activation by secondary M···F interactions.

Conflicts of interest

There are no conflicts to declare.

Acknowledgements

We are grateful to the Royal Society for provision of a University Research Fellowship (MRC) and to the Leverhulme Trust (RPG-2015-248) and ERC (FluoroFix: 677367) for generous funding. Prof. Stuart Macgregor is thanked for insightful discussions and his seminal contributions to the mechanistic analysis of reactions that break C–F bonds.

References

1 W. Chen, C. Bakewell and M. Crimmin, *Synthesis*, 2017, **49**, 810–821.
2 T. Ahrens, J. Kohlmann, M. Ahrens and T. Braun, *Chem. Rev.*, 2015, **115**, 931–972.
3 M. Teltewskoi, J. A. Panetier, S. A. Macgregor and T. Braun, *Angew. Chem., Int. Ed.*, 2010, **49**, 3947–3951.
4 W.-H. Guo, Q.-Q. Min, J.-W. Gu and X. Zhang, *Angew. Chem., Int. Ed.*, 2015, **54**, 9075–9078.
5 X.-W. Liu, J. Echavarren, C. Zarate and R. Martin, *J. Am. Chem. Soc.*, 2015, **137**, 12470–12473.
6 J. Zhou, M. W. Kuntze-Fechner, R. Bertermann, U. S. D. Paul, J. H. J. Berthel, A. Friedrich, Z. Du, T. B. Marder and U. Radius, *J. Am. Chem. Soc.*, 2016, **138**, 5250–5253.
7 T. Niwa, H. Ochiai, Y. Watanabe and T. Hosoya, *J. Am. Chem. Soc.*, 2015, **137**, 14313–14318.
8 S. I. Kalläne, M. Teltewskoi, T. Braun and B. Braun, *Organometallics*, 2015, **34**, 1156–1169.
9 H. Sakaguchi, Y. Uetake, M. Ohashi, T. Niwa, S. Ogoshi and T. Hosoya, *J. Am. Chem. Soc.*, 2017, **139**, 12855–12862.
10 T. Niwa, H. Ochiai and T. Hosoya, *ACS Catal.*, 2017, **7**, 4535–4541.
11 S. Ito, N. Kato and K. Mikami, *Chem. Commun.*, 2017, **53**, 5546–5548.
12 J. Zhang, W. Dai, Q. Liu and S. Cao, *Org. Lett.*, 2017, **19**, 3283–3286.
13 J. Landmann, P. T. Hennig, N. V. Ignat'ev and M. Finze, *Chem. Sci.*, 2017, **8**, 5962–5968.
14 E. Clot, O. Eisenstein, N. Jasim, S. A. Macgregor, J. E. McGrady and R. N. Perutz, *Acc. Chem. Res.*, 2011, **44**, 333–348.
15 H. Amii and K. Uneyama, *Chem. Rev.*, 2009, **109**, 2119–2183.
16 J. Weaver and S. Senaweera, *Tetrahedron*, 2014, **70**, 7413–7428.
17 S. Erhardt and S. A. Macgregor, *J. Am. Chem. Soc.*, 2008, **130**, 15490–15498.
18 A. Nova, S. Erhardt, N. A. Jasim, R. N. Perutz, S. A. Macgregor, J. E. McGrady and A. C. Whitwood, *J. Am. Chem. Soc.*, 2008, **130**, 15499–15511.
19 N. Yoshikai, H. Matsuda and E. Nakamura, *J. Am. Chem. Soc.*, 2009, **131**, 9590–9599.
20 R. B. King, *Acc. Chem. Res.*, 1970, **3**, 417–427.
21 M. I. Bruce and F. G. A. Stone, *Angew. Chem., Int. Ed.*, 1968, **7**, 747–753.
22 B. L. Booth, R. N. Haszeldine and M. B. Taylor, *J. Chem. Soc. A*, 1970, 1974–1975.
23 B. L. Booth, R. N. Haszeldine and I. Perkins, *J. Chem. Soc., Dalton Trans.*, 1975, 1843–1845.
24 G. A. Artamkina, A. Y. Milchenko, I. P. Beletskaya and O. A. Reutov, *J. Organomet. Chem.*, 2017, **311**, 199–206.
25 B. L. Edelbach and W. D. Jones, *J. Am. Chem. Soc.*, 1997, **119**, 7734–7742.
26 T. H. Peterson, J. T. Golden and R. G. Bergman, *Organometallics*, 1999, **18**, 2005–2020.
27 C. Bakewell, A. J. P. White and M. R. Crimmin, *J. Am. Chem. Soc.*, 2016, **138**, 12763–12766.
28 C. Jones, *Nat. Rev. Chem.*, 2017, **1**, 0059.
29 L. Davin, R. McLellan, A. R. Kennedy and E. Hevia, *Chem. Commun.*, 2017, **53**, 11650–11653.
30 Full reference in ESI.†
31 J.-D. Chai and M. Head-Gordon, *J. Chem. Phys.*, 2008, **128**, 84106.
32 P. Fuentealba, L. V. Szentpaly, H. Preuss and H. Stoll, *J. Phys. B: At. Mol. Phys.*, 1999, **18**, 1287–1296.
33 M. Dolg, U. Wedig, H. Stoll and H. Preuss, *J. Chem. Phys.*, 1987, **86**, 866–872.
34 W. J. Hehre, R. Ditchfield and J. A. Pople, *J. Chem. Phys.*, 1972, **56**, 2257–2261.
35 P. C. Hariharan and J. A. Pople, *Theor. Chim. Acta*, 1973, **28**, 213–222.
36 T. Clark, J. Chandrasekhar, G. N. W. Spitznagel and P. V. R. Schleyer, *J. Comput. Chem.*, 1983, **4**, 294–301.
37 J. Tomasi, B. Mennucci and R. Cammi, *Chem. Rev.*, 2005, **105**, 2999–3094.
38 J.-D. Chai and M. Head-Gordon, *Phys. Chem. Chem. Phys.*, 2008, **10**, 6615.
39 A series of functionals were tested and benchmarked against experimental data (activation parameters, molecular coordinates of stationary points). These studies are presented in the ESI.† While the B3PW91 functional most accurately modelled the experimental Gibbs activation energy associated with **TS-1**, the ωB97X functional was not only within a reasonable margin of error for this data point but also captured all the qualitative experimental trends reported herein.
40 C. E. Pitsch and X. Wang, *Chem. Commun.*, 2017, **53**, 8196–8198.
41 Y. Kim, H. Cho and S. Hwang, *Bull. Korean Chem. Soc.*, 2017, **38**, 282–284.

42 T. Mondal, S. De and D. Koley, *Inorg. Chem.*, 2017, **56**, 10633–10643.
43 C. E. Kefalidis, A. Stasch, C. Jones and L. Maron, *Chem. Commun.*, 2014, **50**, 12318–12321.
44 M. W. Bouwkamp, J. de Wolf, I. Del Hierro Morales, J. Gercama, A. Meetsma, S. I. Troyanov, B. Hessen and J. H. Teuben, *J. Am. Chem. Soc.*, 2002, **124**, 12956–12957.
45 M. W. Bouwkamp, P. H. M. Budzelaar, J. Gercama, I. Del Hierro Morales, J. de Wolf, A. Meetsma, S. I. Troyanov, J. H. Teuben and B. Hessen, *J. Am. Chem. Soc.*, 2005, **127**, 14310–14319.
46 Isolation and separation of the reaction products was hindered by the complex Schlenk equilibria which persist even in the presence of a strongly coordinating co-ligand such as pyridine or 4-dimethylaminopyridine (Fig. S7†).
47 The formation of high nuclearity species such as trimers with this ligand system may account for the complex equilibria in play and the difficulty in separation of C–F activation products derived from **2** compared to those from **1**. See ESI† for further details.
48 J. Hicks, E. J. Underhill, C. E. Kefalidis, L. Maron and C. Jones, *Angew. Chem., Int. Ed.*, 2015, **54**, 10000–10004.
49 J. Hicks, C. E. Hoyer, B. Moubaraki, G. Li Manni, E. Carter, D. M. Murphy, K. S. Murray, L. Gagliardi and C. Jones, *J. Am. Chem. Soc.*, 2014, **136**, 5283–5286.
50 I. Resa, E. Carmona, E. Gutierrez-Puebla and A. Monge, *Science*, 2004, **305**, 1136–1138.
51 Y. Wang, B. Quillian, P. Wei, H. Wang, X.-J. Yang, Y. Xie, R. B. King, P. V. R. Schleyer, H. F. Schaefer and G. H. Robinson, *J. Am. Chem. Soc.*, 2005, **127**, 11944–11945.
52 M. P. Blake, N. Kaltsoyannis and P. Mountford, *Chem. Commun.*, 2015, **51**, 5743–5746.
53 C. Cui, H. W. Roesky, H.-G. Schmidt, M. Noltemeyer, H. Hao and F. Cimpoesu, *Angew. Chem., Int. Ed.*, 2000, **39**, 4274–4276.
54 H. Zhu, R. B. Oswald, H. Fan, H. W. Roesky, Q. Ma, Z. Yang, H.-G. Schmidt, M. Noltemeyer, K. Starke and N. S. Hosmane, *J. Am. Chem. Soc.*, 2006, **128**, 5100–5108.
55 C. Ganesamoorthy, D. Blaser, C. Wolper and S. Schulz, *Chem. Commun.*, 2014, **50**, 12382–12384.
56 T. Chu, I. Korobkov and G. I. Nikonov, *J. Am. Chem. Soc.*, 2014, **136**, 9195–9202.
57 M. R. Crimmin, M. J. Butler and A. J. P. White, *Chem. Commun.*, 2015, **51**, 15994–15996.
58 T. Chu, Y. Boyko, I. Korobkov and G. I. Nikonov, *Organometallics*, 2015, **34**, 5363–5365.
59 B. Li, S. Kundu, H. Zhu, H. Keil, R. Herbst-Irmer, D. Stalke, G. Frenking, D. M. Andrada and H. W. Roesky, *Chem. Commun.*, 2017, **53**, 2543–2546.
60 J. Weßing, C. Göbel, B. Weber, C. Gemel and R. A. Fischer, *Inorg. Chem.*, 2017, **56**, 3517–3525.
61 C. Ganesamoorthy, D. Bläser, C. Wölper and S. Schulz, *Organometallics*, 2015, **34**, 2991–2996.
62 S. P. Green, C. Jones and A. Stasch, *Science*, 2007, **318**, 1754–1757.
63 S. J. Bonyhady, C. Jones, S. Nembenna, A. Stasch, A. J. Edwards and G. J. McIntyre, *Chem.–Eur. J.*, 2009, **16**, 938–955.
64 S. Schulz, D. Schuchmann, U. Westphal and M. Bolte, *Organometallics*, 2009, **28**, 1590–1592.
65 S. P. Green, C. Jones and A. Stasch, *Angew. Chem., Int. Ed.*, 2008, **47**, 9079–9083.
66 Attempts to rationally synthesise **4**, by the reaction of **3** with ZnI_2 or ligated zinc-iodides proved unsuccessful. **3** shows no further reactivity towards BDIZn–I at 298 K (Section 4 ESI†).
67 It was not possible to form new species containing Mg–Al bonds by reaction of aluminium(III) diiodide or aluminium (III) dimethyl complexes with **2**.
68 Addition of 10 equiv. of C_6F_6 to a 0.02 M solution of **3** in C_6D_6 resulted in the slow formation of a mixture of compounds and after 5 days the mixture contained 7% [Zn(^{Dipp}BDI)C_6F_5], 7% [^{Mes}BDIMg(μ-F)]$_3$, and 13% [Mg(^{Mes}BDI)(^{Dipp}BDI)] (Fig. S11 and S12†). Attempts to use higher reaction temperatures only led to the accelerated degradation of **3**.
69 Compound **4** also reacts slowly with C_6F_6 to form the same product [Zn(^{Dipp}BDI)C_6F_5].
70 O. Eisenstein, J. Milani and R. N. Perutz, *Chem. Rev.*, 2017, **117**, 8710–8753.
71 S. D. Pike, M. R. Crimmin and A. B. Chaplin, *Chem. Commun.*, 2017, **53**, 3615–3633.
72 S. A. Macgregor, D. McKay, J. A. Panetier and M. K. Whittlesey, *Dalton Trans.*, 2013, **42**, 7386–7395.
73 L. Maron, E. L. Werkema, L. Perrin, O. Eisenstein and R. A. Andersen, *J. Am. Chem. Soc.*, 2005, **127**, 279–292.